Remote Sensing Estimates of Cirrus Particle Size for Tropical and Midlatitude Cirrus : Hexagonal Crystals and Ice Spheres.

Bruce A. Wielicki and Patrick Minnis
Atmospheric Sciences Division
NASA Langley Research Center
Hampton, VA 23681-0001

Robert Arduini and Lindsay Parker
Lockheed Engineering and Sciences Corp.
Hampton, VA 23666

Si-Chee Tsay
Universities Space Research Association
NASA Goddard Space Flight Center
Greenbelt MD 20771

Yoshihide Takano and Kuo-Nan Liou
Department of Meteorology, University of Utah
Salt Lake City, Utah

1. INTRODUCTION

A large discrepancy exists in current estimates of a mean cirrus particle size appropriate for calculations of the effects of these ice clouds on solar and thermal infrared radiative fluxes. For spheres with large size parameter ($x = 2\pi r/\lambda > 30$, where r is particle radius), and moderate absorption ($n^i x < 1$, where n^i is the imaginary index of refraction for ice), the optimal effective particle radius (Hansen and Travis, 1974) is given by:

$$r_e = \int r^3 n(r) dr \,/\, \int r^2 n(r) dr .$$

For the remote sensing of cirrus particle size at wavelengths of 0.83, 1.65, and 2.21μm, a 50μm ice sphere would have a size parameter of about 200, and values of $n^i x$ of 0, 0.045, and 0.06, satisfying the above conditions.

However, while r_e is a well-defined parameter for spheres, this cross-section area-weighted particle radius can only be extended to non-spherical particles by defining some equivalent sphere, typically an equivalent volume or equivalent cross-section area sphere. Using equivalent volume spheres, values of r_e obtained over Lake Michigan on October 28, 1986, during FIRE phase I varied from 200μm (King Air 2D imaging probes) to 60μm (Landsat reflectances at 0.83, 1.65, and 2.2μm, Wielicki et al., 1990), to 25μm (HIS spectrometer thermal emission between 8 and 12μm, Ackerman et al., 1990). Three major uncertainties were identified in this comparison: small ice particles missed by the 2D-C aircraft probes, uncertain ice refractive index, and uncertainties in the single scatter albedos and scattering phase functions used in the radiative calculations.

Since the first FIRE cirrus results, advances have been made in all three areas. The present paper reports on improvements in the radiative modeling of ice particles at 0.83, 1.65 and 2.21 μm wavelengths appropriate for comparisons to Landsat Thematic Mapper data. The paper also includes new results for Landsat observations of ice clouds in the eastern and western tropical Pacific.

2. RADIATIVE MODEL

Radiative transfer calculations used to predict Landsat spectral radiances are performed as outlined in Wielicki et al., 1990 with two exceptions. First, the finite difference radiative transfer method has been replaced by a discrete ordinate method, hereafter termed DISORT (Stamnes et al., 1988; Tsay et al., 1991). The overall accuracy of these two methods,

however, are similar. Second, a hexagonal ice crystal model (Takano and Liou, 1989) is used in the present study for both the single scatter albedo (ω), and scattering phase function (Φ) used in the DISORT calculations. In the earlier study by Wielicki et al., (1990) Mie spheres were used to determine ω, while Φ was taken from laboratory measurements of ice crystals by Volkovitskiy et al. 1980, hereafter denoted as VPP. The VPP phase function was only available for $\lambda = 0.63\mu m$, but was used for all three channels, in the absence of better information. The present study uses phase functions derived for randomly oriented hexagons of width 2a and length L (see Table 1) determined using ray tracing at $\lambda = 0.55$, 1.6, and 2.2μm (Takano and Liou, 1989). Figure 1 shows the hexagonal phase functions for L/2a = 120/60 at all three wavelengths. The figure demonstrates the importance of absorption in reducing the amount of side scattered radiation, as the average imaginary index of refraction for ice increases with wavelength. Table 1 summarizes the radiative modeling differences between the two studies.

TABLE 1. Radiative Modeling Changes

Radiative Model	Scattering Phase Function	Single Scatter Albedo
Current Results:		
Discrete Ordinate	Hexagons, ray tracing: 2a/L = 20/20, 50/40, 120/60, 300/100, 750/160 $\mu m/\mu m$; λ = 0.55, 1.6, 2.2 μm	Hexagons, ray tracing: 2a/L = 20/20, 50/40, 120/60, 300/100, 750/160 $\mu m/\mu m$; 0.83, 1.56 - 1.8, 2.10 - 2.35 μm
Wielicki et al., 1990:		
Finite Difference	Laboratory: 20 μm plates: λ = 0.6 μm only	Mie : r_e = 4, 8, 16, 32, 64, 128μm 0.83, 1.56 - 1.8, 2.10 - 2.35 μm

Figure 2 compares the new hexagonal crystal results for the Landsat 0.83 μm and 1.65 μm channels with the previous VPP/Mie sphere results at a solar zenith angle of 45°. Calculations were performed at 0.83μm extinction optical depths of 0.1, 0.2, 0.5, 1, 2, 3.5, 5, 10, 20, and 50 and are marked by symbols in Figure 2. Takano and Liou (1989) and others have shown that particle absorption efficiency Q_{abs} scales with particle volume. In order to compare with the earlier Mie sphere estimates of Q_{abs}, (which for large particles with $2\pi r/\lambda >> 1$ determines ω) we have given the radius of an equivalent volume sphere for each hexagonal crystal size. Figure 2 shows that for large optical depths the new calculations give results similar to an equivalent volume sphere. At smaller optical depths, however, the changes in the hexagonal scattering phase function with λ (Figure 1) cause larger deviations from the earlier results, so that the hexagonal crystal r_{vol} is as much as a factor of 2 smaller than the VPP/Mie sphere results. In summary, at large optical depths the single scatter albedo dominates the result, and equivalent volume spheres give reasonable results, while at optical depths less than about 10, the λ dependence of the scattering phase function plays a large role.

3. RESULTS

Figure 3 compares the hexagonal crystal predictions for Landsat reflectances at 0.83μm and 1.65μm with Landsat observations. Landsat observations are shown at full spatial resolution of 30 meters, and are uniformly sampled over a set of independent Landsat cloud scenes. Each Landsat scene is a 60 km by 60 km region. The observations are divided into three sets by geographic regions. Figure 3a gives results for 14 Landsat (60 km)^2 scenes taken from the western tropical Pacific near the TOGA/COARE region (13S - 13N, 150E-175E). Figure 3b gives results for 6 scenes from the Eastern Pacific (0N - 13N, 95W-135W). Figure 3c gives results for 5 scenes for northern mid latitudes (30N - 60N, 60W-130W).

Figure 3 shows several interesting characteristics. For all 25 regions, greater than 98% of the observations fall between the 50/40 and 300/100 hexagonal crystal results (r_{vol} between 23 and 78 μm). The median value agrees well with the 120/60 crystal size (r_{vol} = 41 μm). The Eastern Pacific results appear to be bimodal (but no single scene shows both modes). The mid latitude cases and most of the optically thin tropical cirrus (0.83 μm reflectance below 0.2) show a smaller size range of about 50/40 to 120/60. For all data, however, very few observations are found with particle sizes smaller than 50/40. In fact, the

small number of observations following the 20/20 results for the mid latitude cirrus in Figure 3b are supercooled water droplets from the 10/28/86 case in Wielicki et al. (1990).

4. CAVEATS

The great complexity of ice crystal shapes in clouds indicates that even hexagonal crystal interpretations of remotely sensed particle size must be viewed with caution. In particular, studies of the dependence of the scattering phase function on particle shape and imaginary index of refraction are especially important. Final resolution of these issues will require consistency of aircraft, and various remotely sensed particle estimates including near-infrared and thermal infrared radiance techniques, as well as new techniques using multiple wavelength active lidar and radar systems. It should also be noted that the particle sizes inferred from Figure 3 would represent a vertical average over the entire cloud depth for optically thin cloud, while the sizes would represent the microphysical conditions nearer cloud top (optical depth 3-6) for optically thick cloud.

Even with these difficulties, the current results suggest that there might be strong similarities in mid latitude and tropical ice microphysics, at least for optically thin cirrus. Additional cases of mid latitude ice clouds with larger optical depths are needed.

5. REFERENCES

Ackerman, S. A., W. L. Smith, J. D. Spinhirne, and H. E. Revercomb, 1990: The 27-28 October 1986 FIRE IFO Cirrus Case Study: Spectral Properties of Cirrus Clouds in the 8-12μm Window. *MWR*, **118**, 2377-2388.

Hansen, J. E. and L. D. Travis, 1974: Light scattering in planetary atmospheres, *Space Sci. Rev.*, **16**, 527-610.

Stamnes, K., S. C. Tsay, W. Wiscombe, and K. Jayaweera, 1988: Numerically stable algorithm for discrete-ordinate-method radiative transfer in multiple scattering and emitting layered media. *App. Optics*, **24**, 2502-2509.

Takano, Y. and K- N. Liou, 1989, Solar Radiative Transfer in Cirrus Clouds. Part I: Single Scattering and Optical Properties of Hexagonal Ice Crystals. *Jour. Atmos. Sci*, **46**, 3-19.

Tsay, S.-C., G. L. Stephens, and T. J. Greenwald, 1991: An investigation of aerosol microstructure on visual air quality. *Atmos. Environ.*, **25A**, 1039-1053.

Volkovitskiy, O. A., L. N. Pavlova, and A. G. Petrushin, 1980: Scattering of light by ice crystals. *Izv. Atmos. Ocean. Phys.*, **16**, 98-102.

Wielicki, B. A., J. T. Suttles, A. J. Heymsfield, R. M. Welch, J. D. Spinhirne, M-L. C. Wu, S. K. Cox, D. O'C. Starr, L. Parker, and R. F. Arduini, 1990: The 27-28 October 1986, FIRE IFO Cirrus Case Study: Comparison of Radiative Transfer Theory with Observations by Satellite and Aircraft. *MWR*, **118**, 2356-2376.

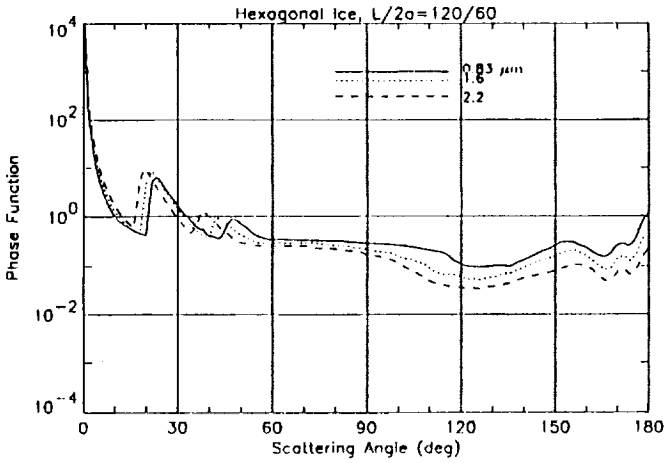

Figure 1

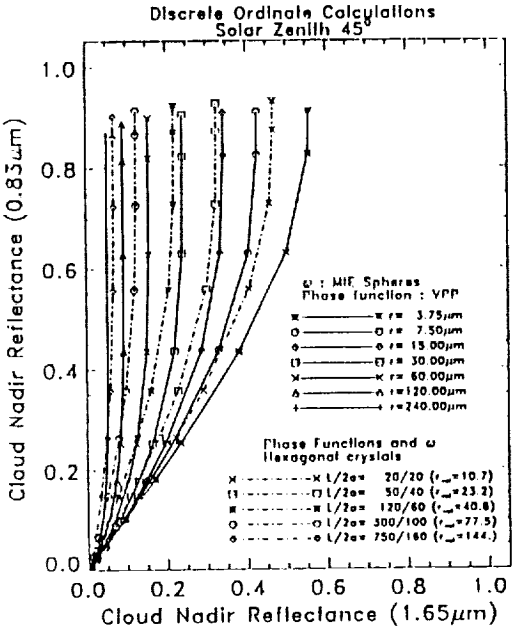

Figure 2

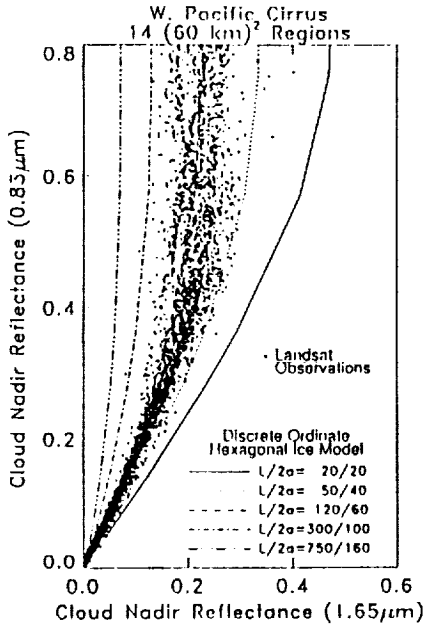

Figure 3a

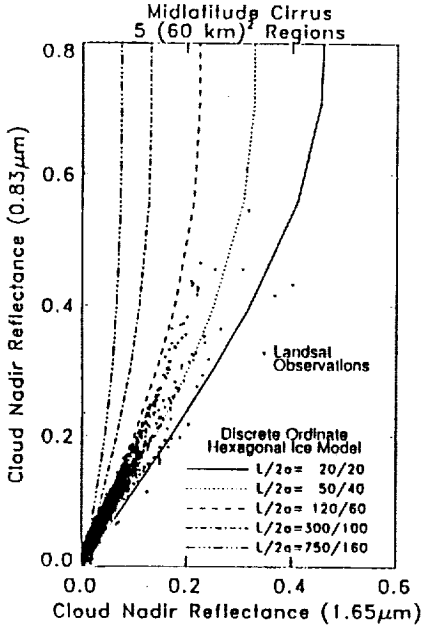

Figure 3c

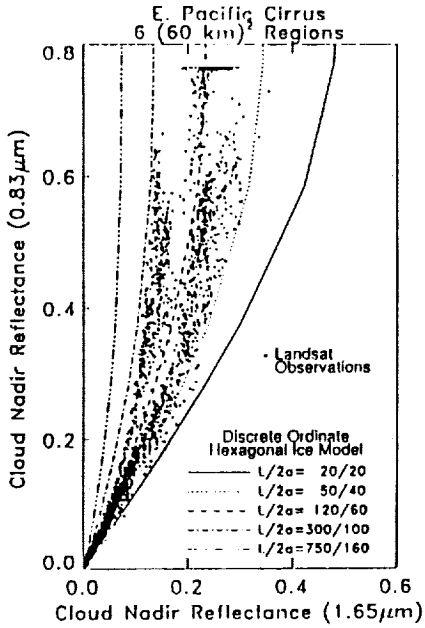

Figure 3b